An Over-Sampling Receiver for Zak-OTFS with Embedded Pilot

Vineetha Yogesh and Ananthanarayanan Chockalingam
Department of ECE, Indian Institute of Science, Bangalore 560012

***Abstract*—Zak-OTFS modulation has emerged as a promising modulation scheme for high-Doppler communication scenarios which are crucial for future wireless systems such as 6G and beyond. In this work, we propose an over-sampling based receiver for Zak-OTFS, where over-sampling is performed in the delay-Doppler (DD) domain. To mitigate the increased processing complexity associated with increased sampling rates, instead of over-sampling the received signal directly, we propose to perform conventional sampling over parallel branches whose inputs are the delay- and Doppler-shifted received signal. This parallel branch sampling (PBS) receiver architecture retains the benefits of over-sampling while significantly reducing computational complexity. We propose a channel estimation and data detection algorithm in the presence of fractional DD for the PBS receiver architecture. We employ the challenging embedded pilot frame structure, in which pilot symbol and data symbols are embedded within a single OTFS frame, leading to pilot-data interference. Our simulation results demonstrate that the proposed PBS receiver architecture enabled by proposed estimation and detection algorithms offers improvements in computational complexity and performance gains in terms of both normalized mean squared error and bit error rate.**

***Index Terms*—OTFS modulation, Zak-OTFS, delay-Doppler domain, embedded pilot, over-sampling, parallel branch sampling.**

I. Introduction

Orthogonal time frequency space (OTFS) modulation is a state-of-the-art modulation that multiplexes information symbols in the delay-Doppler (DD) domain [1], [2]. It effectively handles high Doppler spreads of the channel in high-mobility environments and achieves robust performance. Recently, a new version of OTFS using Zak transform [3], called Zak-OTFS, has been introduced. Zak-OTFS was first introduced in [4], [5], where the authors present the foundational principles and key attributes of Zak-OTFS. They show that Zak-OTFS directly uses the basis functions of the Zak transform for modulation and has the advantages of a formal mathematical framework of using Zak theory to describe the waveform and better performance compared to the earlier multicarrier version of OTFS (MC-OTFS) in [1].

Our focus in this paper is on an over-sampling based low-complexity framework for signal detection and channel estimation in Zak-OTFS. The motivation for the over-sampling framework is presented below. Inspired by the pioneering work in [4], [5], the work in [6] addresses the question of optimal Zak-OTFS receiver for a doubly-selective channel. It shows that a receive (Tx) twisted convolution (TC) filter that is matched to the TC of the physical channel with the transmit (Tx) TC filter, sampled at the DD grid points, is the optimal Zak-OTFS receiver that recovers sufficient statistics for maximum likelihood (ML) detection of the data symbols. Talking about the implementation challenges of this optimal receiver (in Sec. VIII.D, [6]), it points out that when the channel path DD parameters are integer valued and align with the DD grid, the sufficient statistics can be computed from the samples taken on the integer points, and fractional samples are not required. However, when the path parameters are non-integer valued (i.e., fractional DD values), samples taken between the grid points are required to recover the sufficient statistics, and that finer sampling between the grid points (i.e., over-sampling) is required to get accurate measurements of output sample values corresponding to path locations, which can potentially yield more capacity. However, this increases the receiver complexity. The above observations provide the motivation to devise low-complexity algorithms for Zak-OTFS receiver under the over-sampling framework.

Receiver over-sampling in OTFS was first studied in [7] in the context of MC-OTFS, where a modified message passing detection algorithm was proposed for channels with fractional DDs. They demonstrated significant performance improvement over a conventional sampling receiver. Avoiding joint processing of the full over-sampled vector for complexity reasons, the later work in [8], [9] proposed a low-complexity over-sampling receiver based on maximum ratio combining for MC-OTFS. In this paper, we propose a novel over-sampling based receiver for Zak-OTFS using embedded pilot [10] in channels with fractional DDs. In order to reduce the computational complexity resulting due to direct over-sampling of the DD domain received signal, we propose a parallel branch sampling (PBS) receiver architecture, wherein conventional sampling is performed over each branch of the PBS receiver architecture. The input to each branch is the received signal shifted by an appropriate delay and Doppler value that depends on the over-sampling factor. Also, we propose a channel estimation and detection algorithm for the embedded pilot frame using the PBS receiver architecture. It leverages the advantages of over-sampling to provide improved normalized mean squared error (NMSE) and bit error rate (BER) performance by efficiently mitigating the effect of pilot-data interference.

II. Zak-OTFS system model

Figure 1 shows the block diagram of the Zak-OTFS transceiver. MN information symbols from a modulation alphabet $\mathbb{A}$ are embedded on a fundamental DD grid defined as $\Lambda_{\rm dd} = \big\{ (k\Delta\tau, l\Delta\nu) \,\big|\, k=0,\cdots,M-1, l=0,\cdots,N-1 \big\}$, where $\Delta\tau = \frac{1}{B}$ and $\Delta\nu = \frac{1}{T}$ are the resolutions along the delay and Doppler domain, respectively. $B \approx M\nu_p$ is the bandwidth and $T \approx N\tau_p$ is the frame duration, where τ_p and ν_p are fundamental periods along delay and Doppler axis, respectively, such that $\tau_p\nu_p = 1$. The information symbols, denoted by $x[k,l]$s, are encoded as per the following equation

This work was supported in part by the J. C. Bose National Fellowship and the NSF-DST project, Department of Science and Technology, Government of India. The first author would like to thank the Prime Minister's Research Fellowship, Ministry of Education, Government of India for the support.

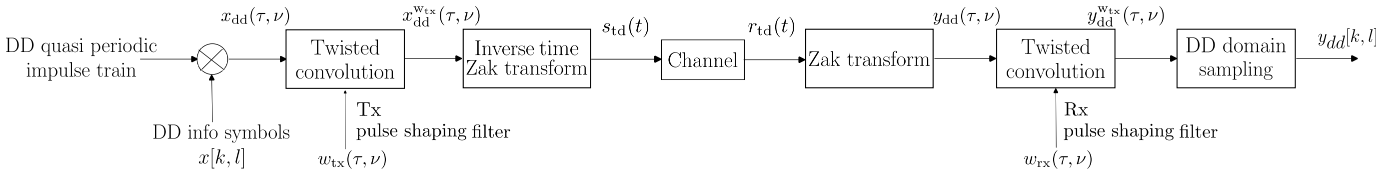

Fig. 1: Block diagram of Zak-OTFS transceiver.

to obtain a quasi-periodic extension of the signal in the discrete DD domain:

$$x_{\rm dd}[k+nM,l+mN]=x[k,l]e^{j2\pi n\frac{l}{N}},n,m\in\mathbb{Z}. \quad (1)$$

The discrete quasi-periodic signal in (1) is converted into a continuous quasi-periodic DD signal by mounting on a continuous quasi-periodic DD impulse train, as

$$x_{\rm dd}(\tau,\nu)=\sum_{k,l\in\mathbb{Z}}x_{\rm dd}[k,l]\delta\left(\tau-k\Delta\tau\right)\delta\left(\nu-l\Delta\nu\right), \quad (2)$$

where $\delta(\cdot)$ denotes the dirac delta function. The signal in (2) is time and bandwidth limited to $\frac{1}{B}$ and $\frac{1}{T}$, respectively, by filtering through the DD domain Tx filter $w_{\rm tx}(\tau,\nu)$, as $x_{\rm dd}^{\rm w_{tx}}(\tau,\nu)=w_{\rm tx}(\tau,\nu)*_\sigma x_{\rm dd}(\tau,\nu)$, where $*_\sigma$ denotes the twisted convolution[1] [5]. The time domain (TD) transmit signal is obtained by using inverse Zak transform as $s_{\rm td}(t)=\mathcal{Z}_t^{-1}\left(x_{\rm dd}^{w_{\rm tx}}(\tau,\nu)\right)=\sqrt{\tau_p}\int_0^{\nu_p}x_{\rm dd}^{w_{\rm tx}}(t,\nu)d\nu$. The transmitted signal passes through a doubly-selective channel having P paths whose DD domain impulse response is

$$h(\tau,\nu)=\sum_{i=1}^{P}h_i\delta(\tau-\tau_i)\delta(\nu-\nu_i), \quad (3)$$

where h_i,τ_i, and ν_i are the channel gain, delay, and Doppler of the ith path, respectively. At the receiver, the TD signal is $r_{\rm td}(t)=\iint h(\tau,\nu)s_{\rm td}(t-\tau)e^{j2\pi\nu(t-\tau)}d\tau d\nu+n(t)$, where $n(t)$ is the additive white Gaussian noise with one-sided power spectral density N_0. Zak transform is used to convert the received TD signal $r_{\rm td}(t)$ to DD domain as

$$\begin{aligned} y_{\rm dd}(\tau,\nu) &= \mathcal{Z}_t(r_{\rm td}(t)) \\ &= \sqrt{\tau_p}\sum_{k\in\mathbb{Z}}r_{\rm td}(\tau+k\tau_p)e^{-j2\pi\nu k\tau_p}+n_{\rm dd}(\tau,\nu), \end{aligned} \quad (4)$$

where $n_{\rm dd}(\tau,\nu)=\mathcal{Z}_t(n(t))$ is the noise in DD domain. Next, $y_{\rm dd}(\tau,\nu)$ is filtered through the Rx DD domain filter $w_{\rm rx}(\tau,\nu)$, which is matched to the Tx DD filter, i.e., $w_{\rm rx}(\tau,\nu)=w_{\rm tx}^*(-\tau,-\nu)e^{j2\pi\tau\nu}$. The output of the Rx DD filter is given by [5]

$$\begin{aligned} y_{\rm dd}^{w_{\rm rx}}(\tau,\nu) &= w_{\rm rx}(\tau,\nu)*_\sigma y_{\rm dd}(\tau,\nu) \\ &= h_{\rm dd}(\tau,\nu)*_\sigma x_{\rm dd}(\tau,\nu)+n_{\rm dd}^{w_{\rm rx}}(\tau,\nu), \end{aligned} \quad (5)$$

where $h_{\rm dd}(\tau,\nu)$ is the effective continuous DD channel (consisting of the cascade of the Tx DD filter, physical DD channel, and Rx DD filter), given by

$$h_{\rm dd}(\tau,\nu)=w_{\rm rx}(\tau,\nu)*_\sigma h(\tau,\nu)*_\sigma w_{\rm tx}(\tau,\nu), \quad (6)$$

[1]Twisted convolution between functions $a(\tau,\nu)$ and $b(\tau,\nu)$ is defined as $a(\tau,\nu)*_\sigma b(\tau,\nu)=\iint_{\mathbb{R}}a(\tau',\nu')b(\tau-\tau',\nu-\nu')e^{j2\pi\nu'(\tau-\tau')}d\tau'd\nu'$.

and $n_{\rm dd}^{w_{\rm rx}}(\tau,\nu)=w_{\rm rx}(\tau,\nu)*_\sigma n_{\rm dd}(\tau,\nu)$ is the filtered noise in the DD domain. Now, let $z(\tau,\nu)$ denote the received information signal in the absence of noise. Using the definition of twisted convolution, $z(\tau,\nu)$ is written as

$$\begin{aligned} z(\tau,\nu) &= h_{\rm dd}(\tau,\nu)*_\sigma x_{\rm dd}(\tau,\nu) \\ &= \iint h_{\rm dd}(\tau',\nu')x_{\rm dd}(\tau-\tau',\nu-\nu')e^{j2\pi\nu'(\tau-\tau')}d\tau'd\nu'. \end{aligned} \quad (7)$$

Substituting (2) in (7), we get

$$z(\tau,\nu)=\sum_{k,l\in\mathbb{Z}}x_{\rm dd}[k,l]h_{\rm dd}(\tau-k\Delta\tau,\nu-l\Delta\nu)e^{j2\pi(\nu-l\Delta\nu)k\Delta\tau}. \quad (8)$$

Using the quasi-periodicity in (1) and restricting the DD indices to $k\in\{0,\ldots,M-1\}$ and $l\in\{0,\ldots,N-1\}$ in (8), we obtain

$$z(\tau,\nu)=\sum_{k=0}^{M-1}\sum_{l=0}^{N-1}x_{\rm dd}[k,l]h_{\rm eff}(\tau,\nu,k,l), \quad (9)$$

where $h_{\rm eff}(\tau,\nu,k,l)$ is given by (10) at the top of next page.

III. Proposed DD domain over-sampling

Conventional sampling has been considered in the Zak-OTFS literature so far, i.e., (5) is sampled on $\Lambda_{\rm dd}$ to obtain MN samples. In this paper, sampling is performed on the received DD domain signal with an over-sampling factor of Q_τ (a resulting sampling rate of $\frac{\Delta\tau}{Q_\tau}$) along delay axis and a factor Q_ν (a resulting sampling rate of $\frac{\Delta\nu}{Q_\nu}$) along Doppler axis. The over-sampling grid is given by

$$\begin{aligned} \Lambda_{\rm dos} &= \Big\{\Big(k'\frac{\Delta\tau}{Q_\tau},l'\frac{\Delta\nu}{Q_\nu}\Big)\Big| \\ & k'=0,1,\ldots,MQ_\tau-1,l'=0,1,\ldots,NQ_\nu-1\Big\}. \end{aligned} \quad (11)$$

Sampling (5) on (11) is referred to as 'direct over-sampling (DOS)'. The resultant samples of the over-sampled signal are

$$z_{\rm dos}[k',l']=\sum_{k=0}^{M-1}\sum_{l=0}^{N-1}x_{\rm dd}[k,l]h_{\rm eff}\left(k'\frac{\Delta\tau}{Q_\tau},l'\frac{\Delta\nu}{Q_\nu},k,l\right). \quad (12)$$

Further, let $n_{\rm dd}^{w_{\rm rx}}[k',l']$ denote the noise samples obtained after sampling $n_{\rm dd}^{w_{\rm rx}}(\tau,\nu)$ on (11). Let The $\mathbf{R}_{\rm dos}\in\mathbb{C}^{MNQ_\tau Q_\nu\times MNQ_\tau Q_\nu}$ denote the covariance matrix of noise whose $[k_1NQ_\nu+l_1,k_2NQ_\nu+l_2]$th element is given by

$$\begin{aligned} \mathbf{R}_{\rm dos}[k_1NQ_\nu+l_1,k_2NQ_\nu+l_2] &= \\ & \mathbb{E}[n_{\rm dd}^{w_{\rm rx}}[k_1,l_1]n_{\rm dd}^{w_{\rm rx}*}[k_2,l_2]], \end{aligned} \quad (13)$$

where $k_1,k_2\in\{0,\ldots,MQ_\tau-1\}$ and $l_1,l_2\in\{0,\ldots,NQ_\nu-1\}$. The samples of the DOS signal are given by

$$\mathbf{y}_{\rm dos}[k'NQ_\nu+l']=z_{\rm dos}[k',l']+n_{\rm dd}^{w_{\rm rx}}[k',l']. \quad (14)$$

$$h_{\text{eff}}(\tau,\nu,k,l) = \sum_{m,n\in\mathbb{Z}} h_{\text{dd}}(\tau-(k+nM)\Delta\tau, \nu-(l+mN)\Delta\nu) e^{j2\pi(\nu-(l+mN)\Delta\nu)(k+nM)\Delta\tau} e^{j2\pi\frac{nl}{N}}. \tag{10}$$

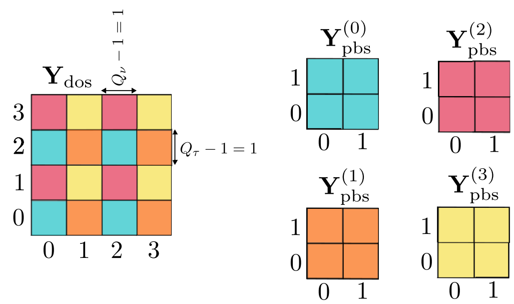

Fig. 2: DOS in the DD domain and partitioning $\mathbf{Y}_{\text{dos}}$ matrix into multiple $\mathbf{Y}_{\text{pbs}}$ matrices.

The DD domain input-output (I/O) relation in matrix-vector form for direct over-sampling can then be written as

$$\mathbf{y}_{\text{dos}} = \mathbf{H}_{\text{dos}}\mathbf{x} + \mathbf{n}_{\text{dos}}, \tag{15}$$

where $\mathbf{y}_{\text{dos}} \in \mathbb{C}^{MNQ_\tau Q_\nu\times 1}, \mathbf{x} \in \mathbb{C}^{MN\times 1}$, $\mathbf{H}_{\text{dos}} \in \mathbb{C}^{MNQ_\tau Q_\nu\times MN}$, and $\mathbf{n}_{\text{dos}} \in \mathbb{C}^{MNQ_\tau Q_\nu\times 1}$, with $\mathbf{x}[kN+l] = x_{\text{dd}}[k,l]$, $\mathbf{H}_{\text{dos}}[k'NQ_\nu + l', kN+l] = h_{\text{eff}}(k'\frac{\Delta\tau}{Q_\tau}, l'\frac{\Delta\nu}{Q_\nu}, k, l)$ given by (16) at the top of the next page, $\mathbf{n}_{\text{dos}}[k'NQ_\nu + l'] = n_{\text{dd}}^{w_{\text{rx}}}[k',l']$, and $\mathbf{y}_{\text{dos}}[k'NQ_\nu + l']$ given by (14). Let $\mathbf{Y}_{\text{dos}}[k,l] = \mathbf{y}_{\text{dos}}[kNQ_\nu + l]$ denote the $MQ_\tau \times NQ_\nu$ received over-sampled matrix used for further processing. Note that by setting $Q_\tau = Q_\nu = 1$, we get the sampling instants corresponding to the case of conventional sampling on Λ_{dd}.

Note that size of $\mathbf{Y}_{\text{dos}}$ grows with increase in Q_τ and Q_ν, thus resulting in increased processing complexity. In order to mitigate the increase in complexity due to over-sampling, we propose partitioning of $\mathbf{Y}_{\text{dos}}$ into $Q_\tau Q_\nu$ blocks (each of size $M\times N$) and further use them for processing at reduced complexity compared to processing $\mathbf{Y}_{\text{dos}}$ as a whole[2].

Let $\mathbf{Y}_{\text{pbs}}^{(q_\tau + Q_\tau q_\nu)}$ denote the $(q_\tau + Q_\tau q_\nu)$th partitioned block of size $M\times N$ for a given q_τ and q_ν, where $q_\tau \in \{0,1,\ldots,Q_\tau-1\}$ and $q_\nu \in \{0,1,\ldots,Q_\nu-1\}$, given by

$$\begin{aligned}\mathbf{Y}_{\text{pbs}}^{(q_\tau+Q_\tau q_\nu)} = \mathbf{Y}_{\text{dos}}[&q_\tau : Q_\tau : MQ_\tau - Q_\tau + q_\tau, \\ &q_\nu : Q_\nu : NQ_\nu - Q_\nu + q_\nu],\end{aligned} \tag{17}$$

where $[a:c:b] = \{a+sc \mid s = 0,1,2,\ldots$ and $a+sc \le b\}$. Figure 2 illustrates the proposed partitioning for a system with $M = N = 2$ and $Q_\tau = Q_\nu = 2$. $\mathbf{Y}_{\text{dos}}$ matrix of size $MQ_\tau \times NQ_\nu$ (i.e., 4×4 matrix in this case) is partitioned into $Q_\tau Q_\nu$ number of $\mathbf{Y}_{\text{pbs}}$ matrices each of size $M\times N$ (i.e., 4 matrices, each of size 2×2) as per (17).

A. Equivalence of proposed partitioning to conventional sampling on parallel branches

The partitioning described above can be viewed as performing conventional sampling on parallel branches where each branch samples a delay- and Doppler-shifted version of the received signal with a delay resolution of $\Delta\tau$ and a Doppler resolution of $\Delta\nu$. The input to the q'th branch, $q' \in \{0,1,\ldots,Q_\tau Q_\nu - 1\}$ is shifted along delay domain by $\frac{q_\tau}{Q}\Delta\tau$ and along Doppler domain by $\frac{q_\nu}{Q_\nu}\Delta\nu$, i.e., the input signal to the q'th branch is $y_{\text{dd}}^{w_{\text{rx}}}(\tau + \frac{q_\tau}{Q_\tau}\Delta\tau, \nu + \frac{q_\nu}{Q_\nu}\Delta\nu)$. Thus, essentially, the sampling instants on the q'th branch have a fixed offset of $\frac{q_\tau}{Q_\tau}$ along delay axis and $\frac{q_\nu}{Q_\nu}$ along Doppler axis. The sampling instants along delay and Doppler axis are thus $(k' + \frac{q_\tau}{Q_\tau})\Delta\tau$ and $(l' + \frac{q_\nu}{Q_\nu})\Delta\nu$, respectively, where $k' = 0,1,\ldots,M-1$ and $l' = 0,1,\ldots,N-1$. Note that these sampling points are fractional in nature. This fractional nature of the sampling points is exploited while formulating the proposed channel estimation algorithm in Sec. IV-A.

The sampled signal obtained from q'th branch by sampling $z(\tau + \frac{q_\tau}{Q_\tau}\Delta\tau, \nu + \frac{q_\nu}{Q_\nu}\Delta\nu)$ (see (9)) on Λ_{dd} is given by

$$\begin{aligned}z^{(q')}[k',l'] = &\sum_{k=0}^{M-1}\sum_{l=0}^{N-1} x_{\text{dd}}[k,l] \\ &h_{\text{eff}}\left(\left(k' + \frac{q_\tau}{Q_\tau}\right)\Delta\tau, \left(l' + \frac{q_\nu}{Q_\nu}\right)\Delta\nu, k, l\right).\end{aligned} \tag{18}$$

Similarly, let $n_{\text{dd}}^{w_{\text{rx}}(q')}[k',l']$ denote the samples of the filtered noise of the q'th branch. Then, the $[k_1N + l_1, k_2N + l_2]$th element of the noise covariance matrix is $\mathbf{R}^{(q')}[k_1N + l_1, k_2N + l_2] = \mathbb{E}[n_{\text{dd}}^{w_{\text{rx}}(q')}[k_1,l_1] n_{\text{dd}}^{w_{\text{rx}}(q')*}[k_2,l_2]]$, where $\mathbf{R}^{(q')} \in \mathbb{C}^{MN\times MN}$, $k_1,k_2 \in \{0,1,\ldots,M-1\}$, and $l_1,l_2 \in \{0,1,\ldots,N-1\}$.

The matrix-vector DD domain I/O relation corresponding to the q'th branch, with parallel branch sampling, is given by

$$\mathbf{y}^{(q')} = \mathbf{H}^{(q')}\mathbf{x} + \mathbf{n}^{(q')}, \tag{19}$$

where $\mathbf{y}^{(q')} \in \mathbb{C}^{MN\times 1}, \mathbf{x} \in \mathbb{C}^{MN\times 1}$, $\mathbf{H}^{(q')} \in \mathbb{C}^{MN\times MN}$, and $\mathbf{n}^{(q')} \in \mathbb{C}^{MN\times 1}$, such that $\mathbf{x}[kN+l] = x_{\text{dd}}[k,l]$, $\mathbf{H}^{(q')}[k'N + l', kN+l] = h_{\text{eff}}((k' + \frac{q_\tau}{Q_\tau})\Delta\tau, (l' + \frac{q_\nu}{Q_\nu})\Delta\nu, k, l)$ given by (20) at the top of next page, $\mathbf{n}^{(q')}[k'N+l'] = n_{\text{dd}}^{w_{\text{rx}}(q')}[k',l']$, and $\mathbf{y}^{(q')}[k'N+l'] = z^{(q')}[k',l'] + n_{\text{dd}}^{w_{\text{rx}}(q')}[k',l']$. Let $\mathbf{Y}^{(q')}$ denote the $M\times N$ matrix corresponding to the q'th branch constructed such that $\mathbf{Y}^{(q')}[k,l] = \mathbf{y}^{(q')}[kN+l]$.

IV. Proposed Algorithms for Detection and Channel Estimation Using Embedded Pilot

This section presents the channel estimation and detection algorithms for the proposed parallel branch sampling architecture, i.e., using $\{\mathbf{Y}^{(q')}\}_{q'=0}^{Q_\tau Q_\nu - 1}$. For the purpose of data detection at the receiver, we need an estimate of the effective channel matrices, i.e., $\{\mathbf{H}^{(q')}\}_{q'=0}^{Q_\tau Q_\nu - 1}$. To facilitate channel estimation, we consider the embedded pilot frame structure (see Fig. 3) defined as [10]

$$\mathbf{X}_{\text{emb}}[k,l] = \begin{cases}\sqrt{E_{\text{p}}} & \text{for } k = k_{\text{p}}, l = l_{\text{p}}, \\ 0 & \text{for } k \in k_{\text{GR}}, l \in l_{\text{GR}}, \\ a\sqrt{\frac{E_{\text{d}}}{N_{\text{d}}}} & \text{otherwise},\end{cases} \tag{21}$$

[2]With LMMSE equalizer, the DOS system has detection complexity of $\mathcal{O}(Q_\tau^3 Q_\nu^3 M^3 N^3)$, while with partitioning it reduces to $Q_\tau Q_\nu \mathcal{O}(M^3N^3)$.

$$\mathbf{H}_{\mathrm{dos}}[k'NQ_\nu + l', kN + l] = \sum_{m,n\in\mathbb{Z}} h_{\mathrm{dd}}\left(k'\frac{\Delta\tau}{Q_\tau} - (k + nM)\Delta\tau, l'\frac{\Delta\nu}{Q_\nu} - (l + mN)\Delta\nu\right) e^{j2\pi\frac{(l'-(l+mN)Q_\nu)(k+nM)}{MNQ_\nu}} e^{j2\pi\frac{nl}{N}}. \tag{16}$$

$$\mathbf{H}^{(q')}[k'N + l', kN + l] = \sum_{m,n\in\mathbb{Z}} h_{\mathrm{dd}}\left(\left(k' + \frac{q_\tau}{Q_\tau} - k - nM\right)\Delta\tau, \left(l' + \frac{q_\nu}{Q_\nu} - l - mN\right)\Delta\nu\right) e^{j2\pi\frac{(l'+\frac{q_\nu}{Q_\nu}-(l+mN))(k+nM)}{MN}} e^{j2\pi\frac{nl}{N}}. \tag{20}$$

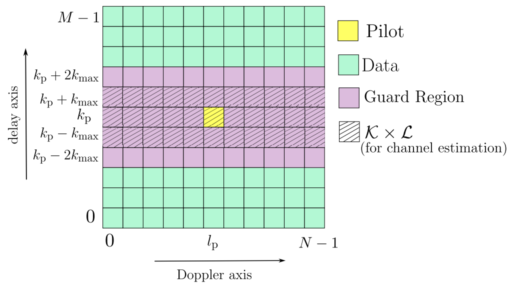

Fig. 3: Embedded pilot frame structure

where $a \in \mathbb{A}$, $(k_\mathrm{p}, l_\mathrm{p})$ is the pilot location in the frame, $k_{\mathrm{GR}} = \{k_\mathrm{p}-2k_{\max}, k_\mathrm{p}-2k_{\max}+1, \cdots, k_\mathrm{p}+2k_{\max}\}\backslash k_\mathrm{p}$ and $l_{\mathrm{GR}} = \{0, 1, \cdots, N-1\}\backslash l_\mathrm{p}$ define the guard regions (GR) around the pilot along delay and Doppler axis, respectively, to mitigate pilot-data interference, where $k_{\max} = \lceil \tau_{\max}/\Delta\tau \rceil$. The number of DD bins used for channel estimation (pilot and GR) are $N_\mathrm{p} = N(4k_{\max}+1)$ and the number of bins used for transmitting data are $N_\mathrm{d} = MN - N_\mathrm{p}$. Thus, the throughput is $\frac{N_\mathrm{d}}{MN}$. Further, E_p and E_d denote the average pilot and data energies, respectively, and $\frac{E_\mathrm{p}}{E_\mathrm{d}}$ denotes the pilot energy to data energy ratio (PDR) [10]. Let the vectors $\{\mathbf{y}_{\mathrm{emb}}^{(q')}\}_{q'=0}^{Q_\tau Q_\nu-1}$ and their matrix forms $\{\mathbf{Y}_{\mathrm{emb}}^{(q')}\}_{q'=0}^{Q_\tau Q_\nu-1}$ denote the output blocks of the proposed multi-branch receiver architecture when $\mathbf{x} = \mathbf{x}_{\mathrm{emb}}$ in (19), where $\mathbf{x}_{\mathrm{emb}}[kN+l] = \mathbf{X}_{\mathrm{emb}}[k, l]$. The input to the channel estimation algorithm is $\{\tilde{\mathbf{Y}}^{(q')} = \mathbf{Y}_{\mathrm{emb}}^{(q')} \odot \mathbf{M}\}_{q'=0}^{Q_\tau Q_\nu-1}$, where $\mathbf{M} \in \{0, 1\}^{M\times N}$ is

$$\mathbf{M}[k, l] = \begin{cases} 1 & \text{for } k \in \mathcal{K}, l \in \mathcal{L}, \\ 0 & \text{otherwise}, \end{cases} \tag{22}$$

where $\mathcal{K} = \{k_\mathrm{p} - k_{\max}, k_\mathrm{p} - k_{\max} + 1, \cdots, k_\mathrm{p} + k_{\max}\}$, $\mathcal{L} = \{0, 1, \cdots, N-1\}$, and $\odot$ denotes Hadamard product. The input to the proposed data detection algorithm is $\{\check{\mathbf{Y}}^{(q')} = \mathbf{Y}_{\mathrm{emb}}^{(q')} \odot (\mathbf{M}+1) \bmod 2\}_{q'=0}^{Q_\tau Q_\nu-1}$.

A. Proposed channel estimation algorithm

The proposed channel estimation using the parallel branch output blocks, i.e., $\{\tilde{\mathbf{Y}}_{\mathrm{emb}}^{(q')}\}_{q'=0}^{Q_\tau Q_\nu-1}$ is listed in **Algorithm 1**. Other inputs are maximum number of estimated paths $P_{\max}$ and threshold $\epsilon = N_\mathrm{p}N_0$, which are used to define stopping criteria. The algorithm is iterative and progresses path-wise, i.e., one path is estimated and canceled in one iteration. For this, we define a temporary matrix $\{\mathbf{W}_j^{(q')}\}_{q'=0}^{Q_\tau Q_\nu-1}$ and corresponding vectors $\{\mathbf{w}_j^{(q')}\}_{q'=0}^{Q_\tau Q_\nu-1}$, where j is the iteration index. In first iteration, i.e., $j = 1$, initialize $\{\mathbf{W}_1^{(q')} = \tilde{\mathbf{Y}}_{\mathrm{emb}}^{(q')}\}_{q'=0}^{Q_\tau Q_\nu-1}$ and $\{\mathbf{w}_1^{(q')} = \tilde{\mathbf{y}}_{\mathrm{emb}}^{(q')}\}_{q'=0}^{Q_\tau Q_\nu-1}$, where $\tilde{\mathbf{y}}_{\mathrm{emb}}^{(q')}[kN+l] = \tilde{\mathbf{Y}}_{\mathrm{emb}}^{(q')}[k, l]$. In jth iteration, a fractional estimate of the path delay and Doppler index, i.e., $\tilde{k}[j]$ and $\tilde{l}[j]$, respectively, are obtained by finding the relative shift of

Algorithm 1 Proposed channel estimation algorithm

1: **Inputs:** Received signal and noise covariance matrices on $Q_\tau Q_\nu$ branches : $\{\tilde{\mathbf{Y}}_{\mathrm{emb}}^{(q')}\}_{q'=0}^{Q_\tau Q_\nu-1}$ and $\{\mathbf{R}^{(q')}\}_{q'=0}^{Q_\tau Q_\nu-1}$, $\mathbf{x}_{\mathrm{emb}}$, maximum number of estimated paths $P_{\max}$, $\epsilon = N_\mathrm{p}N_0$
2: **Initialize:** path index $j = 1$, temporary matrix/vector in 1st iter: $\mathbf{W}_1^{(q')} = \tilde{\mathbf{Y}}_{\mathrm{emb}}^{(q')}$, $\mathbf{w}_1^{(q')} = \tilde{\mathbf{y}}_{\mathrm{emb}}^{(q')}$, $E_{\mathrm{res}} = \frac{\sum_{q'=0}^{Q_\tau Q_\nu-1} ||\mathbf{W}_1^{(q')}||_2^2}{Q_\tau Q_\nu}$
3: **while** $j < P_{\max}$ or $E_{\mathrm{res}} \leq \epsilon$ **do**
4: **for** $q' = 0$ to $Q_\tau Q_\nu - 1$ **do**
5: $\gamma_j^{(q')} = \max_{k\in\{0,\ldots,M-1\}, l\in\{0,\ldots,N-1\}} |\mathbf{W}_j^{(q')}[k, l]|^2$
6: $[k_j^{(q')}, l_j^{(q')}] = \arg\max_{k\in\{0,\ldots,M-1\}, l\in\{0,\cdots,N-1\}} |\mathbf{W}_j^{(q')}[k, l]|^2$
7: **end for**
8: Obtain $\tilde{q} = \arg\max_{q'\in\{0,\ldots,Q_\tau Q_\nu-1\}} [\gamma_j^{(q')}]$, $\tilde{q}_\tau = (\tilde{q})_{Q_\tau}$, $\tilde{q}_\nu = \lfloor \frac{\tilde{q}}{Q_\tau} \rfloor$
9: $\tilde{\mathbf{k}}[j] = k_j^{(\tilde{q})} + \frac{\tilde{q}_\tau}{Q_\tau} - k_\mathrm{p}$, $\tilde{\mathbf{l}}[j] = l_j^{(\tilde{q}_\nu)} + \frac{\tilde{q}_\nu}{Q_\nu} - l_\mathrm{p}$
10: Construct $\mathcal{D}_k = \left[\tilde{\mathbf{k}}[j] - \frac{1}{2Q_\tau} : \frac{1}{(|\mathcal{D}_k|-1)Q_\tau} : \tilde{\mathbf{k}}[j] + \frac{1}{2Q_\tau}\right]$ and $\mathcal{D}_l = \left[\tilde{\mathbf{l}}[j] - \frac{1}{2Q_\nu} : \frac{1}{(|\mathcal{D}_l|-1)Q_\nu} : \tilde{\mathbf{l}}[j] + \frac{1}{2Q_\nu}\right]$
11: Obtain $(\breve{\mathbf{k}}[j], \breve{\mathbf{l}}[j])$ by solving (23)
12: Obtain $(\hat{\mathbf{k}}[j], \hat{\mathbf{l}}[j]) = \begin{cases} (\tilde{\mathbf{k}}[j], \tilde{\mathbf{l}}[j]), \text{no refinement} \\ (\breve{\mathbf{k}}[j], \breve{\mathbf{l}}[j]), \text{with refinement} \end{cases}$
13: Obtain $\hat{\boldsymbol{\tau}}[j] = \hat{\mathbf{k}}[j]\Delta\tau$ and $\hat{\boldsymbol{\nu}}[j] = \hat{\mathbf{l}}[j]\Delta\nu$
14: Obtain $\hat{\mathbf{h}}[j] = (\hat{\boldsymbol{\Gamma}}_j^{(q')^H} \mathbf{R}^{(\tilde{q})^{-1}} \hat{\boldsymbol{\Gamma}}_j^{(q')})^{-1} \hat{\boldsymbol{\Gamma}}_j^{(q')^H} \mathbf{R}^{(\tilde{q})^{-1}} \mathbf{w}_j^{(\tilde{q})}$, where $\hat{\boldsymbol{\Gamma}}_j^{(q')} = \hat{\boldsymbol{\Psi}}_j^{(\tilde{q})}(\hat{\boldsymbol{\tau}}[j], \hat{\boldsymbol{\nu}}[j])$ $(\mathbf{x}_{\mathrm{emb}} \odot \mathbf{m}), \mathbf{m}[kN + l] = \mathbf{M}[k, l])$ and $\hat{\boldsymbol{\Psi}}_j^{(\tilde{q})}(\hat{\boldsymbol{\tau}}[j], \hat{\boldsymbol{\nu}}[j])$ is obtained using (24).
15: Compute jth path contribution as $\hat{\mathbf{y}}_j^{(q')} = \hat{\boldsymbol{\Gamma}}_j^{(q')} \hat{\mathbf{h}}[j]$ and obtain $\hat{\mathbf{Y}}_j^{(q')}[k, l] = \hat{\mathbf{y}}_j^{(q')}[kN + l]$
16: Update residue $\mathbf{W}_{j+1}^{(q')} = \mathbf{W}_j^{(q')} - \hat{\mathbf{Y}}_j^{(q')}$, $\mathbf{w}_{j+1}^{(q')}[kN+l] = \mathbf{W}_{j+1}^{(q')}[k, l]$, and $E_{\mathrm{res}} = \frac{\sum_{q'=0}^{Q_\tau Q_\nu-1} ||\mathbf{W}_{j+1}^{(q')}||_2^2}{Q_\tau Q_\nu}$
17: **update** $j = j + 1$
18: **end while**
19: **Output:** $\hat{\boldsymbol{\tau}}, \hat{\boldsymbol{\nu}}, \hat{\mathbf{h}}$

the maximum energy bin among $\{\mathbf{W}_1^{(q')} = \tilde{\mathbf{Y}}_{\mathrm{emb}}^{(q')}\}_{q'=0}^{Q_\tau Q_\nu-1}$ from $(k_\mathrm{p}, l_\mathrm{p})$ (see lines 4-9 in **Algorithm 1**). If required, the estimates can be further refined by constructing search space around $\tilde{k}[j]$ and $\tilde{l}[j]$ as $\mathcal{D}_k$ along delay axis and $\mathcal{D}_l$ along Doppler axis, respectively (see line 10 in **Algorithm 1**). The fine estimates are obtained as [11]

$$\begin{aligned}(\breve{\mathbf{k}}[j], \breve{\mathbf{l}}[j]) = \arg\max_{\mathcal{D}_k\times\mathcal{D}_l} \Big[&\mathbf{w}_j^{(\tilde{q})^H} \mathbf{R}^{(\tilde{q})^{-1}} \boldsymbol{\Gamma}_j^{(\tilde{q})} \\ &(\boldsymbol{\Gamma}_j^{(\tilde{q})^H} \mathbf{R}^{(\tilde{q})^{-1}} \boldsymbol{\Gamma}_j^{(\tilde{q})})^{-1} \boldsymbol{\Gamma}_j^{(\tilde{q})^H} \mathbf{R}^{(\tilde{q})^{-1}} \mathbf{w}_j^{(\tilde{q})}\Big],\end{aligned} \tag{23}$$

where $\boldsymbol{\Gamma}_j^{(\tilde{q})} = \boldsymbol{\Psi}_j^{(\tilde{q})}(d_k\Delta\tau, d_l\Delta\nu)$ $(\mathbf{x}_{\mathrm{emb}} \odot \mathbf{m}), \mathbf{m}[kN + l] = \mathbf{M}[k, l], \forall\, d_k \in \mathcal{D}_k$ and $d_l \in \mathcal{D}_l$ and $\boldsymbol{\Psi}_i^{(q')}(\tau_i, \nu_i) \in \mathbb{C}^{MN\times MN}$

is the effective channel matrix when the channel has only ith path, given by

$$\mathbf{\Psi}_i^{(q')}(\tau_i,\nu_i) = \mathbf{H}^{(q')} \tag{24}$$
$$\text{with } h_i=1, \tau_u=\nu_u=h_u=0, \forall u\neq i,\ u\in\{1,\ldots,P\}.$$

If refinement is done, then the estimates with refinement (WR), i.e., $((\breve{\mathbf{k}}[j],\breve{\mathbf{l}}[j]))$, are used in the subsequent steps. Otherwise, the estimates with no refinement (NR), i.e., $((\tilde{\mathbf{k}}[j],\tilde{\mathbf{l}}[j]))$, are used[3]. Let $(\hat{\mathbf{k}}[j],\hat{\mathbf{l}}[j])$ denote the final estimates of delay and Doppler indices (see line 12 in **Algorithm 1**). Using $(\hat{\mathbf{k}}[j],\hat{\mathbf{l}}[j])$, obtain an estimate of the channel gain $\hat{\mathbf{h}}[j]$ (see line 14 in **Algorithm 1**) and construct the estimated jth path contribution using $(\hat{\mathbf{h}}[j],\hat{\mathbf{k}}[j],\hat{\mathbf{l}}[j])$ (see line 15 in **Algorithm 1**). Following this, the temporary matrices and vectors are updated and the residual energy E_{res} is computed (see line 16 in **Algorithm 1**). The algorithm progresses until either $E_{\text{res}}<\epsilon$ or $j>P_{\max}$. At the end of the algorithm, the estimated vectors of channel delays, Dopplers, and gains, i.e., $\hat{\boldsymbol{\tau}},\hat{\boldsymbol{\nu}}$, and $\hat{\mathbf{h}}$, respectively, are used to construct the estimated effective channel matrices $\hat{\mathbf{H}}^{(q')}, q'\in\{0,1,\ldots,Q_\tau Q_\nu-1\}$, i.e., $(\hat{\boldsymbol{\tau}},\hat{\boldsymbol{\nu}},\hat{\mathbf{h}})$ gives $\hat{h}(\tau,\nu)$ (using (3)), which gives $\hat{h}_{\text{dd}}(\tau,\nu)$ (using (6)). The samples of $\hat{h}_{\text{dd}}(\tau,\nu)$ gives $\hat{\mathbf{H}}^{(q')}, q'\in\{0,1,\ldots,Q_\tau Q_\nu-1\}$ (using (20)). The estimated $\hat{\mathbf{H}}^{(q')}$ matrices are input to the SSD algorithm in Sec. IV-B for detection.

B. *Proposed symbol-wise selection-based detection algorithm*

For symbol detection, linear minimum mean square error (LMMSE) equalization is performed on each branch. Let $\{\mathbf{y}_{\text{eq}}^{(q')}\}_{q'=0}^{Q_\tau Q_\nu-1}$ denote the equalized signal on the parallel branches. Let $\mathcal{I}=\{[1,\ldots,MN]\odot(\mathbf{m}+1) \bmod 2\}\backslash 0$. For each equalized symbol on the q'th branch, $\mathbf{y}_{\text{eq}}^{(q')}[i], i\in\mathcal{I}$, the symbol from $\mathbb{A}$ having minimum Euclidean distance from $\tilde{\mathbf{y}}^{(q')}[i]$ and the corresponding minimum distance are given by

$$\mathbf{e}^{(q')}[i] = \arg\min_{a\in\mathbb{A}}\{|\mathbf{y}_{\text{eq}}^{(q')}[i]-a|\}, \tag{25}$$

$$\mathbf{d}^{(q')}[i] = \min_{a\in\mathbb{A}}\{|\mathbf{y}_{\text{eq}}^{(q')}[i]-a|\}, \tag{26}$$

respectively, where $|\cdot|$ denotes the absolute value. Using the vector $\left\{\mathbf{d}^{(q')}\right\}_{q'=0}^{Q_\tau Q_\nu-1}$, $\tilde{q}$ is obtained as

$$\tilde{q} = \underset{q'=0,\cdots,Q_\tau Q_\nu-1}{\arg\min}\ \mathbf{d}^{(q')}[i], \tag{27}$$

and ith symbol in the Zak-OTFS frame is detected as $\hat{\mathbf{x}}[i]=\mathbf{e}^{(\tilde{q})}[i]$.

V. Results and discussions

In this section, we present the performance of the proposed detection and channel estimation algorithms in the PBS framework. For this, we consider the following system parameters:

TABLE I: Veh-A channel PDP

Path index (i)	1	2	3	4	5	6
Delay τ_i (μs)	0	0.31	0.71	1.09	1.73	2.51
Path power (dB)	0	-1	-9	-10	-15	-20

$M=12, N=14$, $\nu_p=15$ kHz, $\tau_p=1/\nu_p=6.667$ μs, $B\approx M\nu_p=180$ KHz, $T\approx N\tau_p=0.934$ ms, $\Delta\tau=\frac{1}{B}=5.556\mu$s, $\Delta\nu=\frac{1}{T}=1.0714$kHz and 4-QAM. We consider vehicular A (Veh-A) fractional DD channel model whose PDP is given in Table I with $\tau_{\max}=2.51\mu$s, hence $k_{\max}=\lceil\frac{\tau_{\max}}{\Delta\tau}\rceil=1$ resulting in throughput of about 60%. The path Dopplers are distributed as $\nu_i=\nu_{\max}\cos(\theta)$, $\theta\in\text{Unif}[-\pi,\pi]$, and $\nu_{\max}$ is taken as 815 Hz. For channel estimation, pilot is located at $(k_{\text{p}},l_{\text{p}})=(\frac{M}{2},\frac{N}{2})$. $w_{\text{tx}}(\tau,\nu)=\sqrt{BT}\text{sinc}(B\tau)\text{sinc}(T\nu)$ is the DD domain transmit filter. We consider $Q_\tau=Q_\nu=Q$ in all the simulations. In **Algorithm 1**, we fix $P_{\max}=12$ and $|\mathcal{D}_k|=|\mathcal{D}_l|=7$.

A. *NMSE/BER performance as a function of PDR*

PDR is a key factor in the PBS receiver performance. A low PDR indicates low pilot power leading to a degraded NMSE and hence a degraded BER performance. On the other hand, a high PDR implies high pilot power. As the pilot power increases, the NMSE performance improves. However, at very high PDRs, post equalization residual pilot power outside the guard region dominates the data power, leading to degraded BER performance. The simulation results corroborate these observations, as seen in Figs. 4a and 4b, which show the NMSE and BER performance, respectively, of the proposed PBS receiver as a function of PDR for both conventional sampling ($Q=1$) and over-sampling with a factor of $Q=2$ at a fixed data SNR of 15 dB. In Fig. 4a, the NMSE performance of the proposed channel estimation algorithm with NR and WR is plotted. It is observed that in all the cases, the NMSE performance improves as the PDR increases. In both $Q=1$ and $Q=2$ systems, the performance of the proposed WR algorithm shows a substantial improvement compared to the corresponding performance obtained using the NR algorithm. This is attributed to the search-based optimization performed in steps 10 and 11 of the **Algorithm 1**. Notice that the performance of the NR algorithm with $Q=2$ is very close to that obtained with WR. This highlights the potential of the proposed PBS receiver with over-sampling in acquiring the initial fractional estimates (see step 9 in **Algorithm 1**) that are as good as those obtained using the WR algorithm at a low computational complexity compared to WR. In Fig. 4b, it can be seen that at low PDRs, the BER performance improves as PDR increases due to improved NMSE performance, however, as PDR increases beyond 5 dB for $Q=1$ and 10 dB for $Q=2$, the improvement in NMSE performance does not translate to improvement in BER performance. Based on the observations above, a PDR of 5 dB is fixed for all simulations presented below.

B. *NMSE/BER performance as a function of data SNR*

Figures 5 and 6 show the NMSE and BER performance, respectively, of the PBS receiver as a function of data SNR under NR and WR frameworks, with $Q=1,2$. The performance

[3]WR provides estimates closer to the true value than NR, but at a higher computational complexity due to solving (23). As shown in Sec. V, WR significantly improves performance with conventional sampling. However, NR achieves comparable results with over-sampling, highlighting the proposed PBS scheme's ability to provide good performance with lower complexity.

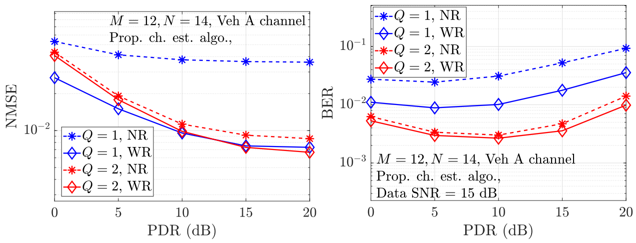

(a) NMSE vs PDR (b) BER vs PDR

Fig. 4: NMSE and BER performance of the proposed PBS receiver as a function of PDR.

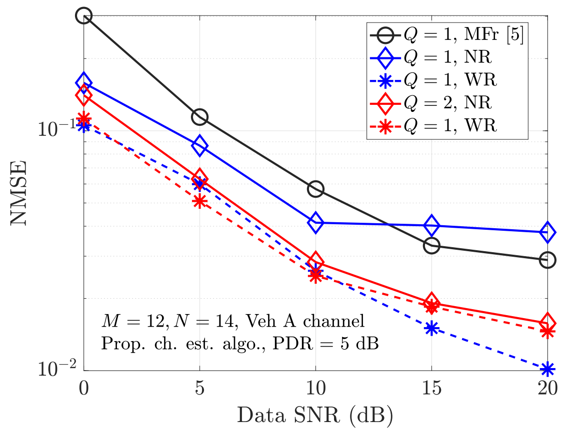

Fig. 5: NMSE performance of the proposed PBS receiver as a function of data SNR.

of the model-free (MFr) channel estimation algorithm in [5] is also plotted for comparison. In Fig. 5, with $Q = 1$ (i.e., integer sampling points), it is observed that the NMSE performance using WR estimates is superior to that obtained using NR estimates and MFr algorithm, thereby emphasizing the need for obtaining fractional estimates of delay and Doppler indices. The MFr algorithm is observed to perform slightly better at high SNRs compared to that with NR estimates. With $Q = 2$, the NMSE performance with NR estimates is very close to that obtained with WR estimates, thus indicating the ability of the proposed PBS architecture to obtain a good initial fractional

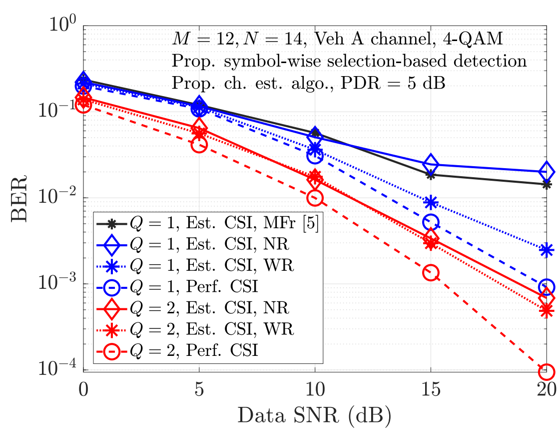

Fig. 6: BER performance of the proposed PBS receiver as a function of data SNR.

estimate. Figure 6 shows the corresponding BER performance. The BER performances with perfect channel state information (CSI) are also plotted for $Q = 1, 2$. It is observed that the BER performance with perfect CSI for $Q = 2$ is superior than that of $Q = 1$. While the MFr and algorithm with NR estimates floor at high SNRs for $Q = 1$, the performance using WR estimates is close to perfect CSI performance. For $Q = 2$, following a similar trend as in NMSE, both WR and NR estimates provide a BER performance close to perfect CSI. The performance with WR estimates is only slightly better than NR algorithm at high SNR. Thus, with over-sampling $(Q > 1)$, the proposed algorithm with NR estimates provides a very good NMSE and BER performance at a low complexity compared to the WR counterpart.

VI. Conclusion

We presented an over-sampling based receiver for Zak-OTFS. We proposed a novel parallel branch sampling based receiver architecture that offered low-complexity processing of the sampled signal compared to the direct over-sampling counter part. An embedded pilot frame was used for the purpose of channel estimation. The work proposed a channel estimation algorithm that uses the fractional nature of the sampling points to obtain the estimates of the path delay and Doppler indices. We also proposed a symbol-wise selection algorithm for data detection that performed LMMSE equalization on parallel branches. Simulation results showed that the proposed receiver achieved good NMSE and BER performance. An over-sampling framework with superimposed pilot which incurs no throughput loss can be investigated further.

References

[1] R. Hadani et al., "Orthogonal time frequency space modulation," *Proc. IEEE WCNC'2017*, pp. 1-6, Mar. 2017.

[2] Z. Wei et al., "Orthogonal time-frequency space modulation: a promising next-generation waveform," *IEEE Wireless Commun. Mag.*, vol. 28, no. 4, pp. 136-144, Aug. 2021.

[3] A. J. E. M. Janssen, "The Zak transform: a signal transform for sampled time-continuous signals," *Philips J. Res.*, 43, pp. 23-69, 1988.

[4] S. K. Mohammed, R. Hadani, A. Chockalingam, and R. Calderbank, "OTFS - a mathematical foundation for communication and radar sensing in the delay-Doppler domain," *IEEE BITS the Inform. Theory Mag.*, vol. 2, no. 2, pp. 36-55, Nov. 2022.

[5] S. K. Mohammed, R. Hadani, A. Chockalingam, and R. Calderbank, "OTFS - predictability in the delay-Doppler domain and its value to communication and radar sensing," *IEEE BITS the Inform. Theory Mag.*, vol. 3, no. 2, pp. 7-31, Jun. 2023.

[6] S. Gopalam, H. Inaltekin, I. B. Collings, and S. V. Hanly, "Optimal Zak-OTFS receiver and its relation to the radar matched filter," *IEEE Open J. of the Commun. Soc.*, vol. 5, pp. 4462-4482, 2024.

[7] Y. Ge, Q. Deng, P. C. Ching and Z. Ding, "Receiver design for OTFS with a fractionally spaced sampling approach", *IEEE Trans. Wireless Commun.*, vol. 20, no. 7, pp. 4072-4086, July 2021.

[8] P. Priya, E. Viterbo and Y. Hong, "Low complexity MRC detection for OTFS receiver with oversampling," *IEEE Trans. Wireless Commun.*, vol. 23, no. 2, pp. 1459-1473, Feb. 2024.

[9] N. Deconda, N. Seshadri, R. D. Koilpillai, "A modified MRC receiver for OTFS systems with oversampling," *IEEE WCNC'2024*, Apr. 2024.

[10] J. Jayachandran et al., "Zak-OTFS: pulse shaping and the tradeoff between time/bandwidth expansion and predictability," *arXiv:2405.02718v1[eess.SP]*.

[11] I. A. Khan and S. K. Mohammed, "A low-complexity OTFS channel estimation method for fractional delay-Doppler scenarios," *IEEE Wireless Commun. Lett.*, vol. 12, no. 9, pp. 1484-1488, Sep. 2023.